Secondary structure of a truncated form of lecithin retinol acyltransferase in solution and evidence for its binding and hydrolytic action in monolayers

ARTICLE *in* BIOCHIMICA ET BIOPHYSICA ACTA · JUNE 2008

Impact Factor: 4.66 · DOI: 10.1016/j.bbamem.2008.01.014 · Source: PubMed

5 AUTHORS, INCLUDING:

Sylvain Bussières
CHU de Québec
9 PUBLICATIONS **88** CITATIONS

SEE PROFILE

Thierry Buffeteau
Université Bordeaux 1
159 PUBLICATIONS **3,780** CITATIONS

SEE PROFILE

Available online at www.sciencedirect.com
ScienceDirect
Biochimica et Biophysica Acta 1778 (2008) 1324–1334
Biochimica et Biophysica Acta BBA
www.elsevier.com/locate/bbamem

Secondary structure of a truncated form of lecithin retinol acyltransferase in solution and evidence for its binding and hydrolytic action in monolayers

Sylvain Bussières [a], Thierry Buffeteau [b], Bernard Desbat [c], Rock Breton [d], Christian Salesse [a,*]

[a] *Unité de recherche en ophtalmologie, Centre Hospitalier Universitaire de Québec, Pavillon CHUL, Département d'ophtalmologie, Faculté de médecine, Université Laval, 2705 Blvd. Laurier, Ste-Foy, Québec, Canada G1V 4G2*
[b] *Institut des Sciences Moléculaires, UMR 5255 du CNRS, Université Bordeaux 1, 351 Cours de la Libération, 33405 Talence, France*
[c] *CBMN, UMR 5248 du CNRS, Université Bordeaux 1, ENITAB, 33607 Pessac, France*
[d] *Unité de recherche en endocrinologie moléculaire, Centre Hospitalier Universitaire de Québec, Pavillon CHUL, Département d'anatomie et physiologie, Faculté de médecine, Université Laval, 2705 Blvd. Laurier, Ste-Foy, Québec, Canada G1V 4G2*

Received 23 November 2007; received in revised form 24 January 2008; accepted 25 January 2008
Available online 7 February 2008

Abstract

Lecithin retinol acyltransferase (LRAT) is a 230 amino acids membrane-associated protein which catalyzes the esterification of all-*trans*-retinol into all-*trans*-retinyl ester. The enzymatic activity of a truncated form of LRAT (tLRAT) which contains the residues required for catalysis but which is lacking N- and C-terminal hydrophobic segments has been shown to depend on the detergent used for its solubilization. Moreover, it is unknown whether tLRAT can bind membranes in the absence of these hydrophobic segments. The present study has allowed to measure the membrane binding and hydrolytic action of tLRAT in lipid monolayers by use of polarization modulation infrared reflection absorption spectroscopy and Brewster angle microscopy. Moreover, the proportion of the secondary structure components of tLRAT was determined in three different detergents by infrared absorption spectroscopy, vibrational circular dichroism and electronic circular dichroism which allowed to explain its detergent dependent activity. In addition, the secondary structure of tLRAT in the absence of detergent was very similar to that in Triton X-100 thus suggesting that, compared to the other detergents assayed, the secondary structure of this protein is very little perturbed by this detergent.

Keywords: Lecithin retinol acyltransferase; Vibrational circular dichroism; Electronic circular dichroism; Infrared spectroscopy; PM-IRRAS; Protein secondary structure

1. Introduction

Lecithin retinol acyltransferase (LRAT) has been shown to be expressed in several tissues including testis, liver, intestine and the retina [1]. It is likely involved in the mobilization and storage of vitamin A [2]. It catalyzes hydrolysis of the *sn*-1 acyl chain of phospholipids and transfers this acyl group to all-*trans* retinol [3–6] to generate all-*trans* retinyl esters. In the retinal pigment epithelium (RPE), these retinyl esters are then further metabolized to produce the chromophore of rhodopsin, 11-*cis* retinal [7]. LRAT is thus an important protein of the visual cycle [8].

The nucleotide sequence of LRAT indicates an open reading frame of 690 bp encoding a 230 amino acid protein with a calculated mass of 25.3 kDa [9]. The primary sequence of LRAT is novel [9] and does not show any homology to enzymes that catalyze similar reactions, such as lecithin cholesterol acyltransferase [10,11]. The analysis of the amino acid sequence of LRAT suggests the existence of N- and C-terminal hydrophobic segments at positions 9–31 and 195–222 [9], respectively, that

Abbreviations: LRAT, Lecithin retinol acyltransferase; VCD, vibrational circular dichroism; ECD, electronic circular dichroism; tLRAT, recombinant truncated form of LRAT; RPE, retinal pigment epithelium; OG, *n*-octyl-β-D-glucopyranoside; SDS, sodium dodecyl sulfate; BSA, bovine serum albumin; DMPC, 1,2-Dimyristoyl-*sn*-Glycero-3-Phosphocholine; cmc, critical micellar concentration; PM-IRRAS, polarization modulation infrared reflection absorption spectroscopy; PC/FA, Principal Component method of Factor Analysis; PLS, Partial Least-Square Analysis; S.D., standard deviation

* Corresponding author. Tel.: +1 418 656 4141x47243; fax: +1 418 654 2131.
E-mail address: Christian.Salesse@crchul.ulaval.ca (C. Salesse).

0005-2736/$ - see front matter © 2008 Elsevier B.V. All rights reserved.
doi:10.1016/j.bbamem.2008.01.014

were postulated to allow membrane binding of LRAT. However, only the C-terminal transmembrane domain has been recently shown to be essential for membrane targeting [12]. It has been reported that the transmembrane domains in the N- and C-terminal regions of the full-length LRAT prevent its purification when expressed in HEK cells [9] as well as in bacteria [13]. A recombinant truncated form of LRAT (tLRAT) (amino acids 31–196) has thus been produced where these hydrophobic segments have been removed [13]. The three essential residues (C161, Y154, and H60) for the activity of LRAT are all conserved in the LRAT family of enzymes [14]. These amino acids are located within the sequence of tLRAT which was thus shown to be fully active [13]. This tLRAT activity is dependent on the detergent used for its solubilization [13]. The amino acids of the active site of tLRAT must interact with membranes to hydrolyze phospholipids. However, information on the membrane binding of tLRAT in the absence of its hydrophobic segments and the effect of detergents on its secondary structure are lacking.

Polarization modulation infrared reflection absorption spectroscopy (PM-IRRAS) overcomes the water absorption limitation using rapid polarization modulation of the incident beam which allows the observation of infrared absorption bands of phospholipids and proteins in monolayers at the air–water interface [15]. Furthermore, it is possible to extract information from the infrared spectra on the kinetics of hydrolysis of monolayers by enzymes using PM-IRRAS [16–18] or IRRAS [19,20]. Brewster angle miscoscopy (BAM) allows to observe the morphology of lipid and lipid–protein monolayers [21,22]. In the present paper, PM-IRRAS has been used to monitor membrane binding and hydrolysis of phospholipid monolayers by tLRAT whereas BAM was used to gain information on the morphology of the resulting protein–lipid monolayer.

Electronic (ECD) and vibrational (VCD) circular dichroism in addition to infrared (IR) absorption spectroscopy allow to probe the secondary structure of proteins for which no structural information is available. It has been shown that ECD is very accurate for α-helix predictions, IR is better for β-sheet estimation and VCD allows a good determination of the different secondary structure components; the latter spectroscopic technique is also very sensitive to random coil structures [23]. Multiple conformations of β-turns make the theoretical calculations very difficult using ECD which can thus lead to a wrong estimation of the relative content in α-helices and β-sheets. VCD measures the rotational strengths of vibrational transitions [24] and is sensitive to short-range order, thus allowing to discriminate β-sheets and all types of helices as well as disordered structures [25]. In the present paper, the effect of detergent on the secondary structure of tLRAT has been determined by infrared absorption spectroscopy, VCD and ECD.

2. Materials and methods

2.1. Materials

The expression vector pET11a and the *Escherichia coli* BL21(DE3)pLysS cells were from Novagen (Madison, WI, USA). The GenElute™ Plasmid Miniprep Kit, Globulin free bovine serum albumin (BSA), EGTA and 1,2-Dimyristoyl-*sn*-Glycero-3-Phosphocholine (DMPC) were from Sigma (St Louis, MO, USA). Amicon 15 concentrators were from Millipore (Beverly, MA, USA). Tris and imidazole were from Laboratoire MAT (Quebec, Canada). EDTA was from Life Technologies (Grand Island, NY, USA). Aprotinin was from Roche Diagnostics (Indianapolis, IN, USA). *n*-octyl-β-D-glucopyranoside was either from Fluka (Sigma-Aldrich, St Louis, MO, USA), Roche Diagnostics (Indianapolis, IN, USA), or A.G. Scientific (San Diego, CA, USA). Triton X-100 was from ICN (Irvine, CA, USA). Sodium chloride was from Ultrapure Bioreagent (Phillipsburg, NJ, USA). IPTG and Sodium dodecylsulfate (SDS) were from Invitrogen (Carlsbad, CA, USA). The anti-LRAT antibody was a generous gift from Dr. Dean Bok (University of California in Los Angeles, CA, USA). The secondary antibody, anti-rabbit IgG (Goat) peroxidase conjugated was from Calbiochem (San Diego, CA, USA). RevertAid H minus First Strand cDNA Synthesis Kit was from Fermentas (Burlington, ON, Canada). Econo-Pac® 10DG columns was from Bio-Rad (Hercules, CA, USA). PhastGel Blue R for Coomassie staining and His-Trap columns were from Amersham Pharmacia (Piscataway, NJ, USA).

2.2. Preparation of LRAT/pET expression vector

The protocol used to clone a truncated form of the human LRAT gene in the vector pET11a was modified from [13]. For the generation of tLRAT, the following set of oligonucleotide primers was used: forward, TGCCATATGGGCAAGGACAAAGGGAGGAACAGT and reverse, AGGCTCAGCTTAGTGATGGTGATGATGATGGTGGTGGTGATGGCTACCACGAGGTACAAGGAGAACACTTCTCTGATCACGAATAAT. tLRAT was amplified by RT-PCR by use of the RPE cDNA template. Briefly, RNA from freshly dissected RPE was isolated by the Tri-reagent method (Sigma) and used for reverse transcription reaction with the RevertAid H minus First Strand cDNA Synthesis Kit. In order to insure unidirectional cloning, additional NdeI and Bpu1102 I restriction sites were attached to the 5′ end of each primer. A His-tag of 10 histidines and a trombin digestion site were also added to the C-terminus (using the reverse primer) to facilitate tLRAT purification. The pET11a vector was then linearized with NdeI and Bpu1102 I and subsequently ligated with the purified PCR product. The generated truncated protein includes amino acids 31 to 196 and contains in total 182 amino acids after adding the His-tag as well as the thrombin digestion site. Its calculated molecular mass is 20.91 kDa. After transformation and production of the recombinant construct in *E. coli* DH5α, plasmid DNA was extracted using GenElute™ Plasmid Miniprep Kit. The positive clones were evaluated by digesting the plasmid with Nde I and Bpu1102 I followed by agarose gel electrophoresis (1.5%). "High flow" sequence analysis using an ABI 3730xl was performed with each construct to confirm the presence, orientation, and correct nucleotide sequence of each DNA insert.

2.3. Expression of tLRAT in bacteria

Plasmid DNA was transformed into *E. coli* Bl21(DE3)pLysS and grown overnight in the LB medium until saturation. Then, fresh LB containing 100 μg/ml ampicillin was inoculated with the transformed culture and incubated at 37 °C under agitation (250 rpm) until $A_{600\ nm}$=0.6. tLRAT expression was then induced with 0.5 mM IPTG followed by an incubation for 6 h at 30 °C. Cells were pelleted by centrifugation at 3720 ×*g* for 20 min and stored at −20 °C.

2.4. Solubilization and purification of histidine-tagged tLRAT

Bacteria were first disrupted by 3 cycles of freeze–thawing in the lysis buffer (Tris 100 mM, NaCl 100 mM, 1 mM EDTA, 1 mM EGTA, 1.4 μg/μl aprotinin, pH 7.8). Cell suspension was then sonicated during 3 min (cycles of 5 s) on ice. Bacteria were then centrifuged at 13,000 ×*g* during 30 min. Supernatant was discarded and membranes were resuspended in the loading buffer (Tris 500 mM, 5 mM imidazole, 0.1% SDS, pH 7.8). The resuspended pellets were shaken overnight at room temperature to homogenize the suspension which was then centrifuged at 100,000 ×*g* for 20 min at 22 °C. The supernatant was then loaded on a 5 ml His-Trap column after equilibration with 5 column volumes of loading buffer. Column was washed with 10 to 20 column volumes of washing buffer (Tris 500 mM, 40 mM imidazole, SDS 0.1%, pH 7.8). Elution was achieved with the elution buffer (Tris 500 mM, 150 mM imidazole, SDS 0.1%, pH 7.8). Alternatively, the SDS used in the washing and elution buffers was changed to 0.1% *n*-octyl-β-D-glucopyranoside (OG), 0.1% CHAPSO or 0.1% Triton

X-100. Fractions containing pure tLRAT were concentrated by centrifugation at 3700 ×*g* at 20 °C using an Amicon 15 device. Concentrated tLRAT was desalted using an Econo-Pac® 10DG column which had been equilibrated with phosphate buffer 10 mM, NaCl 150 mM, pH 7.0 (or carbonate buffer 10 mM, pH 9.2) in the absence or in the presence of either 0.1% SDS, 0.1% OG, 0.1% CHAPSO or 0.1% Triton X-100.

2.5. Electrophoresis, western blot analysis and determination of the concentration of purified tLRAT

After protein separation with 15% SDS-PAGE, proteins were transfered to a nitrocellulose membrane using the transfer buffer (Tris 25 mM, glycine 192 mM). The membrane was blocked with 25 mg/ml globulin free BSA in TBST (25 mM Tris, 0.15 M NaCl, pH 7.6, 0.05% Tween®-20) for 1 h at room temperature. The primary antibody (anti-LRAT, 1:4000 dilution) was then added to the membranes followed by the secondary antibody (anti-rabbit IgG (Goat) peroxidase conjugated (1:8000 dilution)) and the Super Signal West Pico Chemiluminescent Substrate. Because of the presence of detergent in the protein samples, tLRAT concentration (C) was determined using the difference between the absorbance of tLRAT at 280 nm (A_{280}) and that at 260 nm (A_{260}) using the following relation: $C = 1.55A_{280} - 0.76A_{260}$ [26]. The protein concentrations obtained were very consistent with those estimated when the intensity of the bands of tLRAT on SDS-PAGE were compared to those obtained with known amounts of albumin.

2.6. PM-IRRAS measurements of monolayer binding and hydrolysis by tLRAT

The deionized water used for the preparation of the buffer solutions was highly purified with a NANOpure purification apparatus (Barnstead). This water had a resistivity of no less than 18.2 MΩ*cm and a surface tension of 72± 0.1 mN/m at room temperature. PM-IRRAS spectra were measured as previously described [27,28]. Briefly, PM-IRRAS combines Fourier transform mid-IR reflection spectroscopy (FT-IR) with rapid polarization modulation of the incident beam [15,29]. To remove the isotropic contributions from bulk water and water vapor, experimental drifts and to get rid of the dependence on the Bessel function, the spectrum of the phospholipid monolayer in the presence of the adsorbed tLRAT is subtracted with that of the pure phospholipid monolayer (in the absence of tLRAT) to produce the resulting normalized PM-IRRAS spectrum. Each PM-IRRAS spectrum was the result of the co-addition of 600 scans at a resolution of 8 cm^{-1}. Consequently, a typical PM-IRRAS spectrum was obtained after approximately 9 min of acquisition. In these experiments, the subphase used was a carbonate buffer 50 mM at the optimal pH of 9.2 for tLRAT enzymatic activity [14]. Phospholipids were slowly spread at the surface of the buffer until a surface pressure of 15 mN/m was reached. After an equilibration period of 5 min, 50 μg of tLRAT were injected into the 20 ml subphase and surface pressure was monitored during the measurement of the infrared spectra. tLRAT is injected into the subphase with a *S*-like movement of the syringe underneath the entire surface where the phospholipid was spread. By using this procedure, a quick and homogeneous distribution of fluorescently labeled proteins was previously observed. The 50 μg sample of tLRAT containing 0.1% SDS was typically diluted by a factor of at least 1350 upon injection into the subphase. The final concentration of SDS into the subphase was thus in the range of 0.000074% (3.15×10^{-6} M). Although this amount of SDS is very small, in control experiments, a very quick increase in surface pressure could be observed upon injection of the same amount of SDS into the subphase of a monolayer of pure DMPC at 15 mN/m followed by an immediate return to the original surface pressure. The PM-IRRAS spectra of the DMPC monolayer at 15 mN/m before and after the injection of SDS into the subphase are almost identical. It can thus be postulated that the effect of SDS on the DMPC monolayer is very small.

2.7. Brewster angle microscopy imaging of tLRAT binding onto phospholipid monolayers

The monolayer surface was observed by Brewster angle microscopy (BAM) before and at different time intervals after tLRAT injection underneath the DMPC monolayer in the same conditions as those described for the PM-IRRAS measurements. Monolayers can be imaged by BAM at the Brewster angle of incidence using a parallel p polarized laser beam. In the absence of a monolayer, a zero reflectance is obtained. However, in the presence of a monolayer, a change in reflectivity is measured as a result of a change in refractive index and/or thickness of the film [30]. The Brewster angle microscope BAM2plus (NFT, Göttingen, Germany) was equipped with a frequency doubled Nd: YAG laser with a wavelength of 532 nm and a charge-coupled device (CCD) camera as well as a 10X magnification lens. The exposure time, depending on the image luminosity, was adjusted from 20 μs to 2 ms to avoid saturation of the camera. The spatial lateral resolution of the Brewster angle microscope is 2 μm, and the image size is 400 × 650 μm. The BAM images were coded in gray level.

2.8. Preparation of the samples of tLRAT for vibrational and electronic circular dichroism as well as infrared spectroscopy measurements

The buffer used to purify tLRAT with the His-Trap column was exchanged for 10 mM phosphate buffer (pH 7.0) (or 10 mM carbonate buffer, pH 9.2). tLRAT was then concentrated to 20 mg/ml using an Amicon 15 device and lyophilized overnight. These samples were resuspended in a volume of D_2O such that a final concentration of tLRAT of 40 mg/ml was obtained. The final concentration of detergent was: SDS 0.2% (cmc = 0.17–0.23%), OG 0.2% (cmc = 0.67–0.73%), CHAPSO 0.2% (cmc = 0.5%) or Triton X-100 0.2% (cmc = 0.016%). These samples have been used for the vibrational circular dichroism and infrared spectroscopy measurements. When tLRAT was purified in the absence of detergent, the elution buffer was exchanged for 10 mM phosphate buffer (pH 7). However, tLRAT could not be sufficiently concentrated in the absence of detergent to measure infrared and vibrational circular dichroism spectra as it readily precipitates during this procedure. Therefore, this sample was suitable solely for the ECD measurements. The protein concentration for the ECD measurements was lying between 0.4 and 1 mg/ml.

2.9. Infrared spectroscopy and vibrational circular dichroism of LRAT

The infrared and VCD spectra were recorded with a ThermoNicolet Nexus 670 FTIR spectrometer equipped with a VCD optical bench [31]. In this optical bench, the light beam was focused on the sample by a BaF_2 lens (191 mm focal length), passing an optical filter (1850–800 cm^{-1}), a BaF_2 wire grid polarizer (Specac), and a ZnSe photoelastic modulator (Hinds Instruments, Type II/ZS50). The light was then focused by a ZnSe lens (38.1 mm focal length) onto a 1×1 mm^2 HgCdTe detector (ThermoNicolet, MCTA* E6032). Absorption and VCD spectra were recorded at a resolution of 4 cm^{-1}, by coadding 100 scans and 72 000 scans (24 h acquisition time), respectively. Samples were held in a CaF_2 cell with a fixed path length of 45 μm (BioCell™, BioTools). Baseline corrections of the VCD spectra were performed by subtracting the raw VCD spectra of the D_2O buffer. The photoelastic modulator was adjusted for a maximum efficiency at 1600 cm^{-1}. Calculations were performed via the standard ThermoNicolet software, using Happ and Genzel apodization, de-Haseth phase-correction and a zero-filling factor of one. Calibration spectra were recorded using a birefringent plate (CdSe) and a second BaF_2 wire grid polarizer, following an experimental procedure previously described [32]. Finally, the D_2O buffer absorption was subtracted from the absorption spectra. For the sake of comparison, the VCD spectra are scaled such that all samples have their amide I' absorbance maximum equal to 1. The proportion of the different components of the secondary structure of tLRAT has been estimated with a reference data set of VCD and IR spectra of proteins of known structure using an approach similar to that described by Pancoska et al. [33]. In brief, IR and VCD spectra of 20 different globular proteins (hemoglobin, myoglobin, albumin, glutathione *S* transferase, phospholipase A2, cytochrome *c*, triosephosphate isomerase, lysozyme, thermolysin, lactoferrin, papain, ovalbumin, ribonuclease A, ribonuclease S, carbonic anhydrase, α-chymotrypsinogen, α-chymotrypsin, trypsin, elastase, immunoglobulin) have been measured as described above. These proteins were solubilized in D_2O in the absence of detergent, such that a final concentration of 40 mg/ml was obtained. The secondary structure of these proteins has been determined by the DSSP approach using their X-ray diffraction structure data. The predicted structure of these proteins from their VCD spectra has been

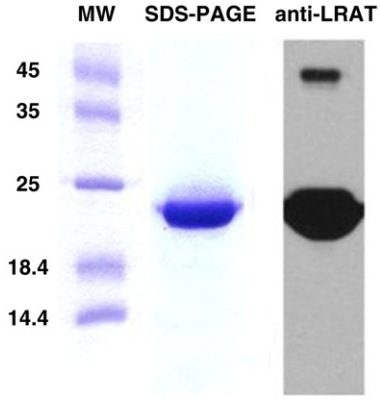

Fig. 1. 15% SDS-PAGE of purified tLRAT in 0.1% OG. Lane 1, standards of molecular weight (kDa); lane 2, purified tLRAT stained with blue coomassie; lane 3, western blot with the anti-LRAT antibody.

calculated using two statistical methods: 1) Principal Component method of Factor Analysis (PC/FA) (a statistical method similar to that published by Pancoska et al. [33]) and 2) Partial Least-Square Analysis (PLS) (TQ Analyst software version 6.2a, ThermoOptek). Results from these two methods are in good agreement (to be published elsewhere). The secondary structure of tLRAT in different detergents has been determined from their VCD and IR spectra with this reference protein data set using the same two methods of statistical analysis which were in good agreement such that only the results obtained using the PC/FA method are presented. Spectra of tLRAT in each of the three different detergents have been measured and the standard deviation was calculated from at least 2 independent expressions and purifications.

2.10. Electronic circular dichroism of LRAT

Electronic circular dichroic (ECD) spectra were recorded on a Jasco Model J-710 spectropolarimeter (Jasco, Easton, MD). The protein concentration has been adjusted to avoid saturation of the detector (the signal was below 600 V between 190 and 200 nm in all experiments except for 0.2% Triton X-100 where the voltage was slightly higher than this value because of the high absorption of this detergent in this region). The buffer contained 10 mM phosphate and either no detergent, 0.1% SDS, 0.1% OG or 0.2% Triton X-100. For each spectrum, 10 scans were collected from 190 to 260 nm using a 0.1 mm pathlenght cuvette for the samples containing detergent whereas a 0.2 mm cuvette was used when tLRAT was purified in the absence of detergent (typically, air bubbles cannot be removed in the 0.1 mm cuvette in the absence of detergent). Spectra of tLRAT in the presence and in the absence of the three different detergents have been measured and the standard deviation was calculated from at least 2 independent expressions and purifications. Secondary structure evaluation has been made using the online software CDSSTR (http://www.cryst.bbk.ac.uk/cdweb/html/home.html) with the protein sets 4, 7 and 8. The software CDSSTR has been selected because it combines the best features of many methods and it is known to perform slightly better than SELCON and CONTIN [34].

3. Results

3.1. Preparation of highly purified tLRAT

Highly purified tLRAT could not be obtained when using an elution buffer containing 500 mM NaCl, as described by Bok et al. [13], because tLRAT eluted at low concentrations of imidazole during the His-Trap chromatography. The use of 500 mM Tris instead of 500 mM NaCl solved this problem. As can be seen in Fig. 1 from the SDS-PAGE electrophoresis and western blot analyses, highly purified tLRAT has been obtained using this procedure. The western blot with the anti-LRAT antibody shows one main band at the expected molecular weight and an additional, much smaller band, at a higher molecular weight (see Fig. 1). The identity of tLRAT in these two bands was further confirmed by mass spectrometry. The higher molecular weight band has been attributed to dimers of tLRAT (~45 kDa) which is consistent with previous observations of Jahng et al. [8].

3.2. Evidence for monolayer binding of tLRAT by PM-IRRAS and Brewster angle microscopy and monolayer hydrolysis by PM-IRRAS

tLRAT is known to catalyze the hydrolysis of the *sn*-1 fatty acyl chain of phospholipids and its transfer to all-*trans* retinol. PM-IRRAS experiments were thus performed to demonstrate monolayer hydrolysis and binding by tLRAT. Fig. 2 shows the PM-IRRAS spectra in the 1000–1800 cm^{-1} region before and after the injection of tLRAT into the monolayer subphase of a pure DMPC monolayer at 15 mN/m. DMPC has been chosen to allow observation of monolayer hydrolysis by tLRAT. Indeed, we have previously shown that the hydrolysis products resulting from phospholipase A2 activity on a DMPC monolayer are readily soluble into the monolayer subphase [35]. Given that the same hydrolysis products are obtained from the tLRAT enzymatic activity (myristic acid and lysomyristoyl phosphatidylcholine), one could expect to observe a decrease of the intensity of the typical infrared bands of DMPC upon monolayer hydrolysis. As can be seen in Fig. 2, the υC=O ester stretching band and the υ_aP=O band of pure DMPC are located at 1735 and 1226 cm^{-1} (see spectrum 1), respectively, which is consistent with previous reports [36]. The intensity of these two bands decreases after the injection of tLRAT into the subphase.

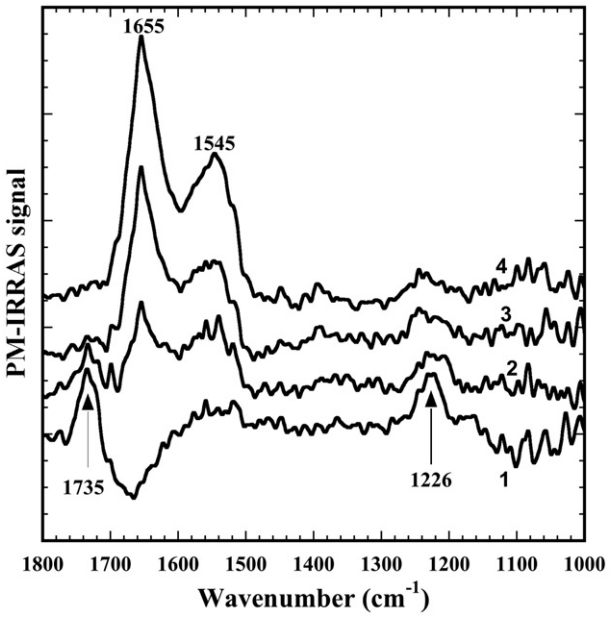

Fig. 2. PM-IRRAS spectra in the 1000–1800 cm^{-1} region of a DMPC monolayer at an initial surface pressure of 15 mN/m (1) before and 2–11 min (2), 21–30 min (3), and 36–45 min (4) after tLRAT injection into the subphase. 50 μg of tLRAT was injected into the subphase containing 25 mL of 50 mM carbonate buffer at pH 9.2.

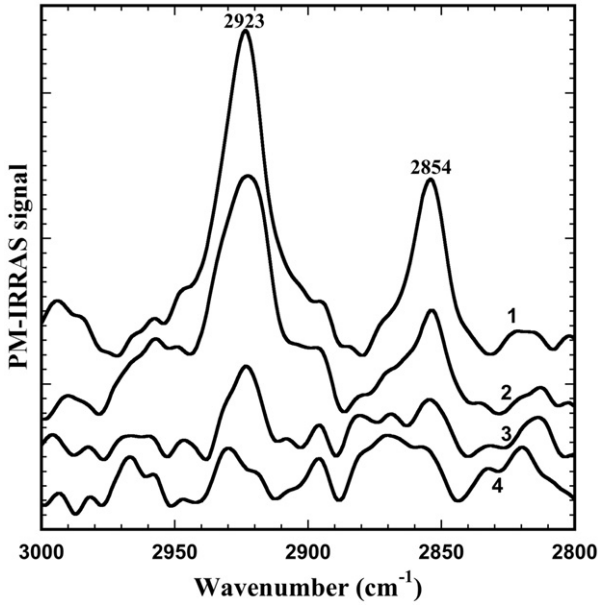

Fig. 3. PM-IRRAS spectra in the 2800–3000 cm^{-1} region of a DMPC monolayer at an initial surface pressure of 15 mN/m before and after tLRAT injection into the subphase. Subphase contains 50 mM carbonate buffer pH at 9.2. Other conditions are the same as in Fig. 2.

The measurement of a PM-IRRAS spectrum lasts for 9 min and, thus, the spectrum is integrated when hydrolysis takes place after the injection of tLRAT underneath the DMPC monolayer. Surface pressure has increased to a stable value of 20 mN/m within this 9 min measuring period of the first spectrum because of tLRAT adsorption. This first spectrum measured soon after tLRAT injection into the subphase (spectrum 2, Fig. 2) shows a significant decrease of the intensity of the C=O ester and P=O bands. Longer adsorption times of tLRAT lead to a much larger extent of monolayer hydrolysis as demonstrated by the further decrease of the intensity of these DMPC infrared bands (spectra 3 and 4, Fig. 2). In parallel to monolayer hydrolysis, the binding of tLRAT onto the DMPC monolayer can be directly observed by the appearance of the amide I and II bands of tLRAT at 1655 and 1545 cm^{-1}, respectively (spectra 2–4, Fig. 2). The position and shape of the amide I band of tLRAT suggests that it contains a significant amount of α-helices as previously observed for other proteins [28,37]. In addition, it can be seen that the more tLRAT is adsorbed, i.e. the larger is the intensity of the amide I and II bands, the more hydrolyzed is the monolayer. The hydrolysis of the DMPC monolayer is further confirmed by the observation of the antisymmetric and symmetric CH_2 stretching bands of the pure DMPC monolayer which are located at 2923 and 2854 cm^{-1}, respectively (spectrum 1, Fig. 3). The position of these bands is consistent with previous observations for DMPC [36]. In agreement with the observation of a decrease of the intensity of the C=O ester and P=O bands (Fig. 2), a similar decrease of the intensity of the CH_2 stretching bands of DMPC as a function of time and extent of tLRAT adsorption (Fig. 3) can be observed which strongly suggests that DMPC monolayer hydrolysis takes place upon tLRAT adsorption.

Fig. 4 shows Brewster angle microscopy images of the DMPC monolayer at 15 mN/m before and after the injection of tLRAT into the subphase. Fig. 4A shows the pure DMPC monolayer. tLRAT was then injected into the subphase and the surface pressure increased to 20 mN/m within 10 min such as in the PM-IRRAS experiments. A lace-like structure (Fig. 4B) can be observed within 5 min after the injection of tLRAT which enventually covers the entire surface of the film (Fig. 4C) and remains unchanged for 2 h. The film was then slowly compressed. It could be seen on the basis of the film movement that the lace-like structure is very rigid. Compression is continued until a surface pressure of 38 mN/m is reached. A highly structured film bearing a flower like shape (Fig. 4D) can then be seen which likely corresponds to protein–lipid multilayers, on the basis of the intensity of the reflectance, that could be made of two-dimensional protein crystals.

3.3. Effect of detergent on the infrared spectra of tLRAT and estimation of the relative proportion of its secondary structure components

Combined bath sonication at 37 °C and vortexing of lyophilized tLRAT purified in CHAPSO did not allow its solubilization with D_2O. The resulting protein suspension was not suitable for IR and VCD analyses. Alternatively, purification of tLRAT in CHAPSO using D_2O was attempted but protein precipitation was observed very quickly after the collection of the fractions. In contrast, solubilization of lyophilized tLRAT purified in SDS, OG or Triton X-100 could readily be achieved at very high concentration (40 mg/ml) in D_2O.

Transmission infrared spectroscopy measurements were performed in solution in order to find out the effect of detergent on the structure of tLRAT. The infrared absorption spectra of tLRAT are presented in Fig. 5. Different spectra are obtained with tLRAT in 0.2% SDS (spectrum 1), 0.2% OG (spectrum 2) and 0.2% Triton X-100 (spectrum 3) with an amide I′ band centered at 1648, 1644 and 1642 cm^{-1}, respectively. The smaller bandwidth of the amide I′ band on the low frequency part of the infrared spectrum of tLRAT in SDS, compared to OG and Triton X-100, together with its position (1648 cm^{-1}) indicates a higher content of α-helices and a lower percentage of β-sheets in this detergent [38,39]. Measurements using tLRAT purified with SDS have also been performed in the presence of palmitic acid, palmitic acid and retinol as well as at two different pHs (7.2 and 9.2). Almost exactly the same spectra, as that shown in Fig. 5 for SDS (see spectrum 1), have been obtained in these conditions. The larger bandwidth of the spectrum of tLRAT in OG and Triton X-100 suggests a larger content in β-sheets in these detergents than in SDS which is clearly demonstrated with the difference spectrum shown in inset A of Fig. 5 where spectrum 1 (SDS) has been subtracted from spectrum 3 (Triton X-100). Indeed, bands at 1623 and 1680 cm^{-1} can be seen in this spectrum which are typical of anti-parallel β-sheets [38,39]. Moreover, the inset B of Fig. 5 shows a shift of 3 cm^{-1} for only tLRAT in OG when infrared spectra are measured before and after the VCD measurements.

As shown in Table 1, the percentage of secondary structure of tLRAT in SDS, OG and Triton X-100 has been estimated from their infrared spectra with the PC/FA method of statistical analysis

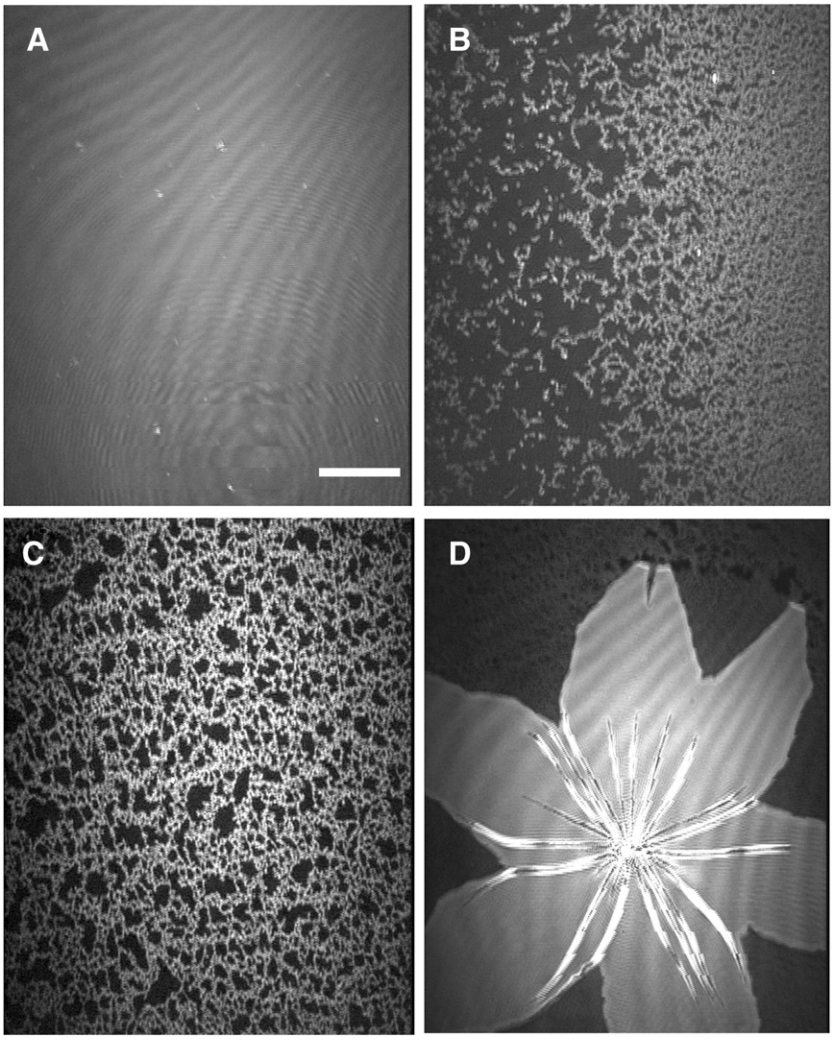

Fig. 4. Brewster angle microscopy imaging of the DMPC monolayer before and after the injection of tLRAT into the subphase. (A) Pure DMPC monolayer. (B) 5 min after the injection of tLRAT. (C) 2 h after the injection of tLRAT (similar images were obtained between 10 min and 2 h after the injection of tLRAT). (D) DMPC–tLRAT film compressed to 38 mN/m. The scale bar shown in Fig. 4A corresponds to 100 μm and is valid for all micrographs. Other conditions are the same as in Fig. 2.

using a reference protein data set (see Section 2.9). The small standard deviation (S.D.) observed reflects the high reproducibility of the measurements. As can be seen in Table 1, tLRAT in OG and Triton X-100 have a very similar secondary structure content as suggested qualitatively from their similar infrared spectra (Fig. 5), except for the content in α-helices. In contrast, tLRAT in SDS contains a smaller percentage of β-sheets and a larger content of β-turns and other conformations (unordered structures) which is consistent with the smaller banwidth and the position of its amide I' band (spectrum 1, Fig. 5) when compared to tLRAT in OG and Triton X-100 (spectra 2 and 3, respectively, Fig. 5).

The infrared spectra contain additional interesting information. Indeed, the bands centered at 1584 and 1515 cm^{-1} can be attributed to the amino acid side chains of Arg $\upsilon_s(CN_3H_5^+)$ and Asp $\upsilon_{as}(COO^-)$ (1584 cm^{-1}) as well as Tyr (Tyr–OH, υ(CC), δ(CH)) (1515 cm^{-1}) in D_2O (Fig. 5) (for a review on the attribution of protein infrared bands in D_2O, see [38]). No difference in the intensity of the band at 1515 cm^{-1} has been observed between tLRAT in the three different detergents used (Fig. 5) whereas a significant difference between the intensity of the infrared band at 1584 cm^{-1} can be seen for tLRAT in Triton X-100 compared to SDS and OG (Fig. 5). The band at 1730 cm^{-1} observed solely for the spectra measured in OG and Triton X-100 (Fig. 5) cannot be attributed to C=O ester groups of phospholipids since no typical band in the CH region (2800–3000 cm^{-1}) can be observed in these spectra (result not shown). This υ(C=O) band can be attributed to the acidic form of Asp and Glu [38,39]. It has been suggested that the environment in the vicinity of the Asp or Glu residues plays a dominant role in stabilizing either the protonated, neutral form or the deprotonated, charged form of these amino acids [38]. It can thus be postulated that tLRAT in SDS contains no acidic form of Asp and Glu in contrast to tLRAT in OG or Triton X-100 and, thus, that tLRAT has a structure in SDS different from that in OG and Triton X-100 which is consistent with the quantitative analysis of the spectra (see Section 3.4). The observation of infrared bands for these amino acid side chains is consistent with the

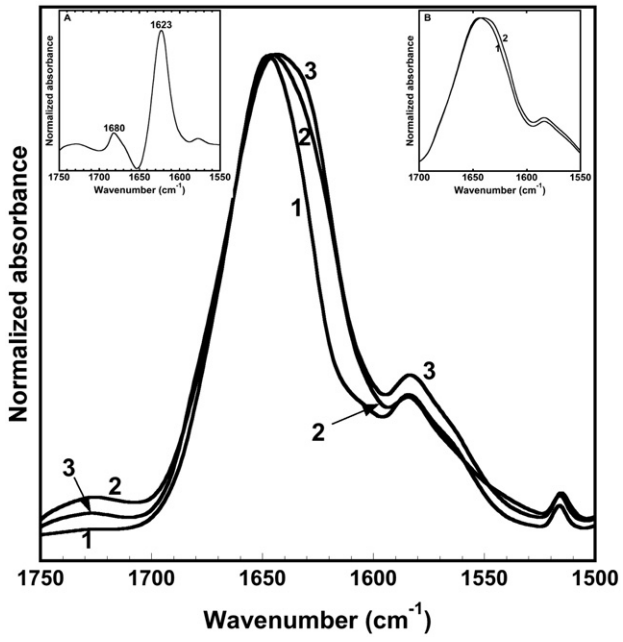

Fig. 5. Infrared absorption spectra of tLRAT in D_2O purified in 0.2% SDS (spectrum 1), 0.2% OG (spectrum 2) and 0.2% Triton X-100 (spectrum 3). The inset A shows a difference spectrum in the amide I′ region where spectrum 1 (SDS) was subtracted from spectrum 3 (Triton X-100). The inset B shows the amide I' band of tLRAT in OG before (spectrum OG1) and after (spectrum OG2) the measurements of the VCD spectra which is typical of 3 independent purifications.

high content of these amino acids in the primary structure of tLRAT (Arg=12, Glu=10, Asp=11, Tyr=7).

3.4. Estimation of the relative proportion of the secondary structure components of tLRAT by vibrational circular dichroïsm

The VCD spectra of tLRAT in SDS, OG and Triton X-100 are presented in Fig. 6. All spectra show negative components at ~1664 and ~1630 cm^{-1} and a positive component at ~1650 cm^{-1}. It is noteworthy that almost exactly the same spectra are obtained for tLRAT in SDS at two different pH (7.2 and 9.2) and in the presence of palmitate or all-*trans* retinol and palmitate (spectra not shown). However, the shape of the VCD spectra depends on the detergent used. Indeed, the band at ~1665 cm^{-1} has a stronger intensity than that at ~1630 cm^{-1} for tLRAT purified in SDS (spectrum 1) and OG (spectrum 2) although the ratio of the intensity between these two bands is stronger in SDS than in OG. This contrasts with the spectrum of tLRAT purified in Triton X-100 where the opposite figure can be observed (spectrum 3, Fig. 6). Indeed, the intensity of the band at 1630 cm^{-1} is stronger than that at 1665 cm^{-1}. These data are qualitatively consistent with a higher content in α-helices for tLRAT in SDS and OG than in Triton X-100 and a higher level of β-sheets in OG and Triton X-100 than in SDS.

These spectra can be quantitatively analyzed to estimate the relative proportion of the different components of the secondary structure of tLRAT (see Table 2) by use of the PC/FA statistical method of analysis using a reference protein data set (see Section 2.9). It can first be seen that similar percentages of β-turns, bend and other conformations are obtained for tLRAT in SDS, OG and Triton X-100 (Table 2). Moreover, a larger content in α-helices but a similar percentage of β-sheets is observed when tLRAT is solubilized in OG compared to Triton X-100. However, a significantly larger content in α-helices and a lower percentage of β-sheets can be seen for tLRAT in SDS compared to OG and Triton X-100 (Table 2). Very similar relative percentages of secondary structure components have been obtained with tLRAT solubilized in SDS in all experimental conditions assayed (data not shown). In fact, the small S.D. reflects the high reproducibility of these different experimental conditions (Table 2). A larger S.D. has been obtained only for the content in α-helices and other conformations in OG. Altogether, the results of these analyses are consistent with the qualitative pattern of the VCD spectra of tLRAT measured in these detergents (Fig. 6). The quantitative analysis of the VCD

Table 1
Estimation of the percentage of the secondary structure components of tLRAT in different detergents from the infrared spectra

	α-helices	β-sheets	β-turns	bend	ρ
SDS (0.2%)	41±1*	16±1	14±0.3	9±0.4	20±0.7
OG (0.2%)	40±0.8	24±2	11±0.4	10±0.2	15±0.5
Triton X-100 (0.2%)	37±0.6	25±0.4	11±0.4	11±1	16±0.4

ρ: other conformations.
*standard deviation calculated from at least 2 independent expressions and purifications.

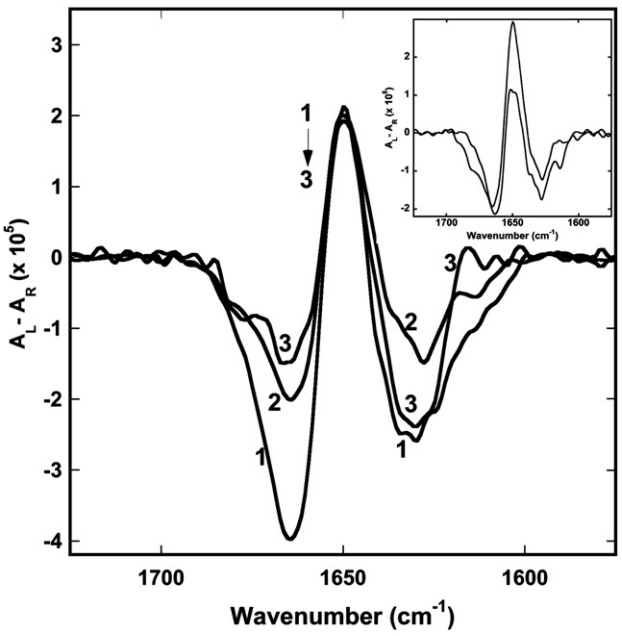

Fig. 6. VCD spectra of tLRAT in D_2O purified in 0.2% SDS (spectrum 1), 0.2% OG (spectrum 2) and 0.2% Triton X-100 (spectrum 3). Spectra 1 and 3 in SDS and Triton X-100, respectively, are typical, highly reproducible spectra. Spectrum 2 is the average spectrum of tLRAT in OG. The inset shows the two most different VCD spectra of tLRAT in OG. VCD spectra are scaled so that all samples have their amide I' absorbance maximum equal to 1.

Table 2
Estimation of the percentage of the secondary structure components of tLRAT in different detergents from the VCD spectra

	α-helices	β-sheets	β-turns	bend	ρ
SDS (0.2%)	42±1*	18±0.9	15±0.5	6±0.1	19±1
OG (0.2%)	37±3	24±0.3	14±0.5	9±0.1	16±2
Triton X-100 (0.2%)	33±0.4	25±0.2	15±0.3	8±0.2	19±0.4

ρ: other conformations.
*standard deviation calculated from at least 2 independent expressions and purifications.

Table 3
Estimation of the percentage of the secondary structure components of tLRAT in different detergents from the ECD spectra

	α-helices	β-sheets	β-turns	random
SDS (0.1%)	44±0*	13±1	16±0.7	27±1
OG (0.1%)	39±5	17±3	16±0.5	28±0.8
Triton X-100 (0.2%)	33±0.1	19±0.1	17±0.1	31±0.2
No detergent	33±2	18±2	17±0	32±0.7

*standard deviation calculated from at least 2 independent expressions and purifications.

and infrared spectra to estimate the relative proportion of each secondary structure component of tLRAT result in quite similar data (compare Tables 1 and 2). Indeed, only a smaller content in α-helices and a larger content in β-turns is obtained for OG and Triton X-100 from the VCD (Table 2) compared to the analysis of the IR spectra (Table 1).

3.5. Estimation of the relative proportion of the secondary structure components of tLRAT by electronic circular dichroism

The ECD measurements performed with tLRAT purified with 0.1% SDS (spectrum 1), 0.1% OG (spectrum 2), 0.2% Triton X-100 (spectrum 3) and in the absence of detergent (spectrum 4) are presented in Fig. 7. The intensity of the spectra of tLRAT in Triton X-100 and in the absence of detergent is lower than those in OG and SDS which is consistent with the lower content in α-helices observed by VCD with Triton X-100

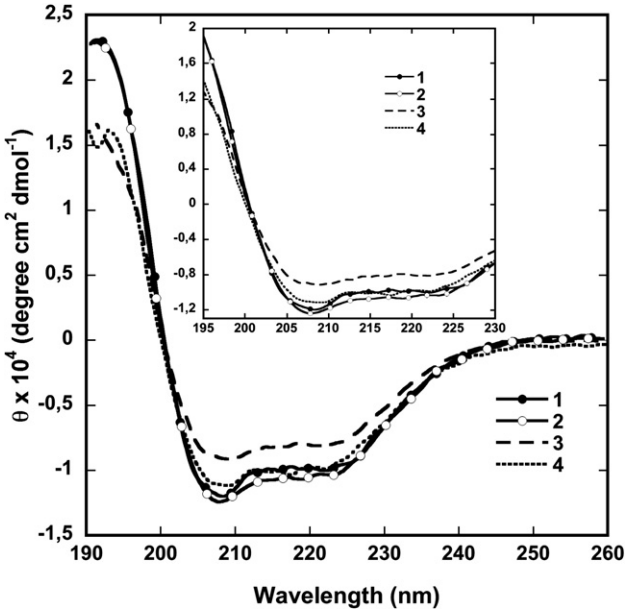

Fig. 7. ECD spectra of tLRAT in H_2O purified in 0.1% SDS (0.8 mg/ml, spectrum 1, —●—), 0.1% OG (0.75 mg/ml, spectrum 2, —○—), 0.2% Triton X-100 (1 mg/ml, spectrum 3, ▬ ▬ ▪) and no detergent (0.7 mg/ml, spectrum 4, ▪▪▪▪▪▪▪▪▪). The region between 195 and 230 nm has been expanded in the inset to more clearly distinguish the different spectra.

(Fig. 6). Highly reproducible spectra of tLRAT have been obtained in Triton X-100, SDS and in the absence of detergent when different purifications are compared (data not shown). In contrast, the intensity of the spectra of tLRAT purified in OG varied from one purification to the other. This is better demonstrated when the spectra are quantitatively analyzed using the CDSSTR software to estimate the relative proportion of each secondary structure component of tLRAT (see Table 3). The small S.D. observed reflects the high reproducibility of the measurements except for OG. Indeed, the S.D. obtained for the percentage of α-helices and β-sheets with tLRAT purified in OG is much larger than that calculated with the other detergents or in the absence of detergent. Therefore, when taking into account this S.D., the percentage of α-helices and β-sheets of tLRAT in OG can be very close to those of tLRAT in either SDS and Triton X-100. Moreover, it can be seen that the percentage of the secondary structure components of tLRAT in SDS and OG are very similar (when taking the S.D. into account) which is consistent with the pattern of their ECD spectra. However, these values are quite different from those obtained for tLRAT in Triton X-100 as well as in the absence of detergent. Indeed, a significantly smaller percentage of α-helices and a larger proportion of β-sheets has been estimated for tLRAT in Triton X-100 and in the absence of detergent compared to SDS and OG. This is also consistent with the qualitative pattern of their ECD spectra presented in Fig. 7. The very similar values obtained for the relative proportion of the secondary structure components of tLRAT in Triton X-100 and in the absence of detergent suggest that the structure of tLRAT is very little perturbed in this detergent when compared to SDS and OG. It is difficult to compare the data obtained by ECD, VCD and IR because ECD cannot distinguish the bend from other conformations. However, if one assumes that the random conformations estimated by ECD include the bend and other conformations calculated from by the VCD and IR spectra, it can be seen that the same general trend is measured by all three methods. Indeed, tLRAT in SDS contains a larger percentage of α-helices, a smaller content of β-sheets and a quite similar percentage of β-turns and random compared to Triton X-100 whereas tLRAT in OG is typically lying in between (compare Tables 1, 2 and 3). Nevertheless, it is noteworthy that the absolute values obtained are not so far from each other even though very different methods are used. ECD has the particular advantage that structural information can be obtained with much lower concentrations of proteins compared to VCD and

IR which allowed the determination of the secondary structure of tLRAT in the absence of detergent.

4. Discussion

The gene encoding LRAT has been only recently cloned [9] and a recombinant truncated form of the protein has then been successfully expressed [13]. The full-length sequence of LRAT has not yet been successfully expressed and purified presumably because of its N- and C-terminal hydrophobic segments. It can be assumed that the C-terminal hydrophobic segment, which is essential for the membrane targeting of LRAT [12], allows to anchor and properly orient LRAT with respect to the membrane which could thus favor its membrane hydrolytic activity. Since LRAT hydrolyzes the *sn*-1 acyl chain of phospholipids, the active site of LRAT located between the N- and C-terminal hydrophobic segments must have access to the membrane. We have expressed and purified tLRAT (lacking the N- and C-terminal hydrophobic segments) to study its binding and hydrolytic action towards lipid monolayers and to probe its structure in solution.

The hydrolytic activity of tLRAT in monolayers has been confirmed by infrared spectroscopic measurements. Indeed, when DMPC hydrolysis takes place, myristic acid and lysomyristoyl phosphatidylcholine are produced. These hydrolysis products are known to be soluble and, thus, the decrease of the intensity of their typical infrared bands (CH_2 stretching, C=O ester and P=O infrared bands; see Figs. 2 and 3) clearly demonstrates that tLRAT actively hydrolyzes the DMPC monolayer. Moreover, the increased intensity of the amide I and II bands of tLRAT with time (spectra 2–4, Fig. 2) demonstrates that an increasing amount of protein binds monolayers. In addition, the observation of the lace-like structures by Brewster angle microscopy (Fig. 4) further demonstrates the monolayer binding of tLRAT. Therefore, the present results demonstrate that the absence of the N- and C-terminal hydrophobic segments does not prevent tLRAT membrane binding and membrane substrate hydrolysis.

Surfactants are widely used to study and handle proteins. SDS is an ionic detergent that is often used because it allows to solubilize hydrophobic proteins. Alternatively, the non-ionic detergents OG and Triton X-100 are commonly used because they do not typically perturb protein structure and are generally considered well suited to study physiological functions of proteins [40–43]. In particular, OG has several advantages over other non-ionic detergents such as Triton X-100 because of its high cmc of 0.67–0.73% which facilitates its removal by dialysis [44]. As mentioned above, the activity of tLRAT was shown to be dependent on the detergent used for its solubilization [13]. Indeed, a lower activity has been measured in SDS whereas the highest activity was obtained with Triton X-100 and CHAPSO. tLRAT activity in OG has not yet been assayed. A relationship can be drawn between the fractional secondary structure of tLRAT and its activity. Indeed, one could postulate that a lower α-helical and a higher β-sheets content such as that measured in 0.2% Triton X-100 (see Tables 1, 2 and 3) is necessary to obtain a high tLRAT activity. Although 1% Triton X-100 has been used by [13] compared to 0.2% in the present study, both measurements were performed above the cmc.

The observation of a higher percentage of α-helices for tLRAT in SDS compared to OG or Triton X-100 (see Tables 1, 2 and 3) is not very surprising. Indeed, for example, two peptides of human apolipoprotein C-I lacking a well-defined structure in aqueous solution adopt a helical, ordered structure upon addition of SDS [45] and this detergent increased the α-helix content of microglobulin-related amyloid fibrils [46] and intact and cleaved α-lactalbumin [47].

The high content in α-helices for tLRAT in OG, which is close to that measured in SDS (see Tables 1, 2 and 3), was rather surprising in view of its well regarded milder properties in maintaining protein structure. However, OG was shown to inactivate some membrane proteins and to dramatically inhibit the activity of glutamante dehydrogenase [48]. In addition, OG was shown to have a strong effect on the conformation of the N-terminal (1–44) domain of human apolipoprotein A-I where an increase of its α-helical content was observed with the increase in the concentration of OG [49]. In addition, when infrared spectra are measured before and after the VCD measurements, a shift of 3 cm^{-1} was only observed for OG, suggesting the formation of β-sheets (see inset B of Fig. 5). Indeed, the spectra of tLRAT in SDS and Triton X-100 remained almost unchanged during the 24 h of acquisition time of the VCD spectra at room temperature. Moreover, two highly different VCD spectra of tLRAT in OG are shown in the inset of Fig. 6. This contrasts with the high reproducibility of the VCD spectra in SDS and Triton X-100. These data, together with the observed variability of the ECD spectra of tLRAT in OG and the much larger standard deviation obtained with OG than with SDS and Triton X-100 (see Tables 2 and 3), argue in favor of the instability of tLRAT in this detergent.

The analysis of the VCD and ECD spectra uses a statistical approach based on the known structure of a reference data set of proteins. Although one can hardly expect to get exactly the same absolute values with both methods, similar values of the structure components and consistent data should be obtained when comparing ECD and VCD results. There is a good agreement between the percentages of secondary structure components obtained by VCD (Table 2) and ECD (Table 3) for tLRAT purified in SDS, OG and Triton X-100 except for the content of β-sheets and, to a much lower extent, of other conformations. Indeed, a larger content in β-sheets is obtained by VCD than by ECD. It has been previously proposed that VCD predicts the β-sheet component better than does ECD [23]. Given that both methods provide similar percentages of α-helices, one could postulate that the secondary structure composition estimated by VCD is more appropriate than that determined by ECD.

Finally, the previous observation of a much lower activity of tLRAT in SDS compared Triton X-100 [13] can thus be explained by the dependence of the secondary structure of this protein in these detergents. Moreover, the high similarity between the secondary structure of tLRAT in the absence and the presence of Triton X-100 suggests that this detergent has no detectable effect on the structure of this protein and thus that it

is most appropriate for functional studies compared to SDS and OG.

Acknowledgements

The work described here was supported by the Natural Sciences and Engineering Research Council of Canada (NSERC). CS is a Chercheur boursier national of the Fonds de la Recherche en Santé du Québec (FRSQ). The Banque d'Yeux Nationale is partly supported by the Réseau de Recherche en Santé de la Vision from the FRSQ. CS also acknowledges support from the Centre National de la recherche scientifique during his sabbatical leave at the Université de Bordeaux.

References

[1] A. Ruiz, D. Bok, Molecular characterization of lecithin-retinol acyltransferase, Methods Enzymol. 316 (2000) 400–413.
[2] A. Ruiz, M.H. Kuehn, J.L. Andorf, E. Stone, G.S. Hageman, D. Bok, Genomic organization and mutation analysis of the gene encoding lecithin retinol acyltransferase in human retinal pigment epithelium, Invest. Ophthalmol. Vis. Sci. 42 (2001) 31–37.
[3] R.J. Barry, F.J. Canada, R.R. Rando, Solubilization and partial purification of retinyl ester synthetase and retinoid isomerase from bovine ocular pigment epithelium, J. Biol. Chem. 264 (1989) 9231–9238.
[4] P.N. MacDonald, D.E. Ong, Evidence for a lecithinretinol acyltransferase activity in the rat small intestine, J. Biol. Chem. 263 (1988) 12478–12482.
[5] R.R. Rando, The biochemistry of the visual cycle, Chem. Rev. 101 (2001) 1881–1896.
[6] J.C. Saari, D.L. Bredberg, Lecithin: retinol acyltransferase in retinal pigment epithelial microsomes, J. Biol. Chem. 264 (1989) 8636–8640.
[7] J. Saari, Biochemistry of visual pigment regeneration, Invest. Ophthalmol. Vis. Sci. 41 (2000) 337–348.
[8] W.J. Jahng, E. Cheung, R.R. Rando, Lecithin retinol acyltransferase forms functional homodimers, Biochemistry 41 (2002) 6311–6319.
[9] A. Ruiz, A. Winston, Y-H. Lim, B.A. Gilbert, R.R. Rando, D. Bok, Molecular and biochemical characterization of lecithin retinol acyltransferase, J. Biol. Chem. 274 (1999) 3834–3841.
[10] O.L. Francone, C.J. Fielding, Structure-function relationships in human lecithin:cholesterol acyltransferase. Site-directed mutagenesis at serine residues 181 and 216, Biochemistry 30 (1991) 10074–10077.
[11] O.L. Francone, C.J. Fielding, Effects of site-directed mutagenesis at residues cysteine-31 and cysteine-184 on lecithin–cholesterol acyltransferase activity, Proc. Natl. Acad. Sci. 88 (1991) 1716–1720.
[12] A.R. Moise, M. Golczak, Y. Imanishi, K. Palczewski, Topology and membrane association of lecithin: retinol acyltransferase (LRAT), J. Biol. Chem. 282 (2006) 2081–2090.
[13] D. Bok, A. Ruiz, O. Yaron, W.J. Jahng, A. Ray, L. Xue, R.R. Rando, Purification and characterization of a transmembrane domain-deleted form of lecithin retinol acyltransferase, Biochemistry 42 (2003) 6090–6098.
[14] L. Xue, R.R. Rando, Roles of cysteine 161 and tyrosine 154 in the lecithinretinol acyltransferase mechanism, Biochemistry 43 (2004) 6120–6126.
[15] T. Buffeteau, B. Desbat, J.M. Turlet, Polarization modulation FT-IR spectroscopy of surfaces and ultra-thin films: experimental procedure and quantitative analysis, Appl. Spectrosc. 45 (1991) 380–389.
[16] M. Grandbois, B. Desbat, D. Blaudez, C. Salesse, Polarization-modulated infrared absorption spectroscopy measurement of phospholipid monolayer hydrolysis by phospholipase, Langmuir 15 (1999) 6594–6597.
[17] M. Grandbois, B. Desbat, C. Salesse, Monitoring of phospholipid monolayer hydrolysis by phospholipase A2 by use of polarization-modulated Fourier transform infrared spectroscopy, Biophys. Chem. 88 (2000) 127–135.
[18] X. Wang, S. Zheng, Q. He, G. Brezesinski, H. Mohwald, J. Li, Hydrolysis reaction analysis of L-alpha-distearoylphosphatidylcholine monolayer catalyzed by phospholipase A2 with polarization-modulated infrared reflection absorption spectroscopy, Langmuir 21 (2005) 1051–1054.
[19] A. Gericke, H. Hühnerfuss, IR reflection absorption spectroscopy: a versatile tool for studying interfacial enzymatic processes, Chem. Phys. Lipids 74 (1994) 205–210.
[20] J. Zheng, B. Desbat, V.K. Rastogi, S.S. Shah, J.J. Defrank, R.M. Leblanc, Organophosphorus hydrolase at the air–water interface: secondary structure and interaction with paraoxon, Biomacromolecules 7 (2006) 2806–2810.
[21] S.M. Hénon, J. Meunier, Microscope at the brewster angle: direct observation of first-order phase transitions in monolayers, Rev. Sci. Instrum. 62 (1991) 936–939.
[22] D. Hönig, D. Möbius, Direct visualization of monolayers at the air–water interface by Brewster angle microscopy, J. Phys. Chem. 95 (1991) 4590–4562.
[23] P. Pancoska, E. Bitto, V. Janota, M. Urbanova, V.P. Gupta, T.A. Keiderling, Comparison of and limits of accuracy for statistical analyses of vibrational and electronic circular dichroism spectra in terms of correlations to and predictions of protein secondary structure, Protein Sci. 4 (1995) 1384–1401.
[24] T.A. Keiderling, Peptide and Protein Conformational Studies with Vibrational Circular Dichroism and Related Spectroscopies, Circular Dichroism: Principles and Applications, vol. 2, 2000, pp. 621–666.
[25] T.A. Keiderling, Protein and peptide secondary structure and conformational determination with vibrational circular dichroism, Curr. Opin. Chem. Biol. 6 (2002) 682–688.
[26] E. Layne, Methods Enzymol. 3 (1957) 447–454.
[27] J. Gallant, B. Desbat, D. Vaknin, C. Salesse, Polarization-modulated infrared spectroscopy and x-ray reflectivity of photosystem II core complex at the gas–water interface, Biophys. J. 75 (1998) 2888–2899.
[28] H. Lavoie, B. Desbat, D. Vaknin, C. Salesse, Structure of rhodopsin in monolayers at the air–water interface: a PM-IRRAS and X-ray reflectivity study, Biochemistry 41 (2002) 13424–13434.
[29] D. Blaudez, J.M. Turlet, J. Dufourcq, D. Bard, T. Buffeteau, B. Desbat, Investigations at the air/water interface using polarization modulation IR spectroscopy, J. Chem. Soc., Faraday. Trans. 92 (1996) 525–530.
[30] D. Vollhardt, Phase transition in adsorption layers at the air–water interface, Adv. Colloid Interface Sci. 79 (1999) 19–57.
[31] T. Buffeteau, F. Lagugne-Labarthet, C. Sourisseau, Vibrational circular dichroism in general anisotropic thin solid films: measurement and theoretical approach, Appl. Spectrosc. 59 (2005) 732–745.
[32] L.A. Nafie, D.W. Vidrine, L.R. Ferraro, L.J. Basile, In fourier transform infrared spectroscopy, Eds (Academic Press, New York) 3 (1982) 83–123.
[33] P. Pancoska, S.C. Yasui, T.A. Keiderling, Statistical analyses of the vibrational circular dichroism of selected proteins and relationship to secondary structures, Biochemistry 30 (1991) 5089–5103.
[34] N. Sreerama, R.W. Woody, Circular Dichroism of Peptides and Proteins, Circular Dichroism: Principles and Applications, vol. 2, 2000, pp. 601–620.
[35] D.W. Grainger, A. Reichert, H. Ringsdorf, C. Salesse, D.E. Davies, J.B. Lloyd, Mixed monolayers of natural and polymeric phospholipids: structural characterization by physical and enzymatic methods, Biochim. Biophys. Acta 1022 (1990) 146–154.
[36] J. Saccani, S. Castano, F. Beaurain, M. Laguerre, B. Desbat, Stabilization of phospholipid multilayers at the air–water interface by compression beyond the collapse: a BAM, PM-IRRAS, and molecular dynamics study, Langmuir 20 (2004) 9190–9197.
[37] F. Wu, C.R. Flach, B.A. Seaton, T.R. Mealy, R. Mendelsohn, Stability of annexin V in ternary complexes with Ca2+ and anionic phospholipids: IR studies of monolayer and bulk phases, Biochemistry 38 (1999) 792–799.
[38] A. Barth, The infrared absorption of amino acid side chains, Prog. Biophys. Mol. Biol. 74 (2000) 141–173.
[39] E. Goormaghtigh, V. Raussens, J.M. Ruysschaert, Attenuated total reflection infrared spectroscopy of proteins and lipids in biological membranes, Biochim. Biophys. Acta 1422 (1999) 105–185.

[40] R.A. Henselman, M.A. Cusanovich, The characterization of sodium cholate solubilized rhodopsin, Biochemistry 13 (1974) 5199–5203.
[41] S. Makino, J.A. Reynolds, C. Tanford, The binding of deoxycholate and Triton X-100 to proteins, J. Biol. Chem. 248 (1973) 4926–4932.
[42] H.B. Osborne, C. Sardet, A. Helenius, Bovine rhodopsin: characterization of the complex formed with Triton X-100, Eur. J. Biochem. 44 (1974) 383–390.
[43] M. Zorn, S. Futterman, Extraction, regeneration after bleaching, and ion-exchange chromatography of rhodopsin in Tween 80, Arch. Biochem. Biophys. 157 (1973) 91–99.
[44] J. Cordoba, M.D. Reboiras, M.N. Jones, Interaction of *n*-octyl-B-D-glucopyranoside with globular proteins in aqueous solution, Int. J. Biol. Macromol. 10 (1988) 270–276.
[45] A. Rozek, G.W. Buchko, R.J. Cushley, Conformation of two peptides corresponding to human apolipoprotein C-I residues 7–24 and 35–53 in the presence of sodium dodecyl sulfate by CD and NMR spectroscopy, Biochemistry 34 (1995) 7401–7408.
[46] S. Yamamoto, K. Hasegawa, I. Yamaguchi, S. Tsutsumi, J. Kardos, Y. Goto, F. Gejyo, H. Naiki, Low concentrations of sodium dodecylsulfate induce the extension of beta 2-microglobulin-related amyloid fibrils at a neutral pH, Biochemistry 43 (2004) 11075–11082.
[47] S. Hamada, Y. Moriyama, K. Yamaguchi, K. Takeda, Conformational stability of alpha-lactalbumin missing a peptide bond between Asp66 and Pro67, J. Protein. Chem. 13 (1994) 423–428.
[48] S. Ghobadi, S. Safarian, A.A. Moosavi-Movahedi, B. Ranjbar, Octyl glucoside induced formation of the molten globule-like state of glutamate dehydrogenase, J. Biochem. (Tokyo) 130 (2001) 671–677.
[49] H.L. Zhu, D. Atkinson, Conformation and lipid binding of the N-terminal (1–44) domain of human apolipoprotein A-I, Biochemistry 43 (2004) 13156–13164.